International Journal for Housing Science and Its Applications
Publish August 6, 2025. Volume 46, Issue 3 Pages 7325-7335

https://doi.org/10.70517/ijhsa463628

Research on digital wrist rehabilitation equipment based on multi-sensor fusion technology

Peijie Liu[1] and Yushi Hu[1,*]
[1] School of Sports Medicine and Health, Chengdu Sport University, Chengdu, Sichuan, 641419, China
Corresponding authors: (e-mail: 19982089416@163.com).

Abstract Aiming at the rehabilitation needs of patients with wrist dysfunction, this study proposes a digital wrist rehabilitation device based on multi-sensor fusion technology. A multimodal data acquisition and fusion framework was constructed by combining surface electromyographic signals and joint motion angle information. The improved WVPSO algorithm is used to optimize the LSSVM hyperparameters to achieve high-precision classification and recognition of finger-wrist movement intentions. Based on ADAMS simulation platform, a virtual prototype model of the device is established to verify its kinematic consistency and human-computer interaction adaptability. The clinical effect of the device was evaluated through a randomized controlled trial of 50 patients with chronic wrist dysfunction. After treatment, the pain, grip strength, function, and dorsal extension/palmar flexion mobility scores of the two groups improved compared with those before treatment, and the mean values of the experimental group were higher than those of the control group by 3.09, 2.41, 4.01, and 3.84 points, respectively. Physical, somatic, and emotional-social scores of the two groups improved compared with the pre-treatment, and the mean values of the experimental group were higher than those of the control group by 8.71, 9.01, 9.83, and 9.32 points, respectively, and the differences were statistically significant ($P<0.05$).

Index Terms wrist rehabilitation, surface EMG signal, WVPSO algorithm, LSSVM algorithm

I. Introduction

Multi-sensor fusion is a technology that synthesizes data from several different types of sensors [1], [2]. Sensor fusion technology, in simple terms, is to combine many different types of sensors together, so that they work together and give play to their respective advantages, so as to obtain more comprehensive and accurate information [3]-[5]. In real life, multi-sensor fusion technology has many application scenarios, such as the field of intelligent security, self-driving cars, etc. With the further development and application of multi-sensor fusion technology, it also plays an important role in healthcare [6]-[9].

In the medical field, multi-sensor fusion technology can be used for the diagnosis and treatment of diseases [10]. For example, in cardiac monitoring, combining data from ECG sensors, blood pressure sensors, heart rate sensors, etc., can provide a more comprehensive understanding of a patient's heart health and provide a more accurate diagnosis basis for doctors [11]-[13]. Injuries to the wrist joint are very common in medical treatment [14]. As an important joint on the human body, the wrist joint is responsible for many movements in daily life [15], [16]. However, due to various reasons, the wrist joint may be injured or otherwise restricted, requiring rehabilitation to restore function [17], [18]. And by applying digital rehabilitation equipment incorporating multi-sensor fusion technology, it can contribute to a better recovery of the wrist joint, based on diversified sensors and intelligent algorithms, which can take the movement data of the wrist injured person at the time and make an accurate feedback through analysis in order to take follow up recovery measures [19]-[22].

This paper firstly introduces the specific structure of the digital wrist rehabilitation equipment, focusing on analyzing the hardware structure of the control system and the software design of the two modules. The relevant action muscle tissue is selected and the EMG signal is preprocessed, and the LSSVM classifier is used to classify and recognize the finger-wrist action. The WVPSO-LSSVM algorithm is proposed to realize the optimization of hyperparameters and provide technical support for wrist rehabilitation equipment. Taking 50 patients with chronic wrist dysfunction in the rehabilitation department as experimental subjects, signal synchronous acquisition and signal pre-processing were carried out. The simulation model of the wrist joint rehabilitation equipment was established based on ADAMS simulation software, and the effectiveness of the design was explored through virtual prototype simulation. The application effect of the wrist rehabilitation equipment was evaluated through a 6-week controlled experimental validation.

II. Design of digital wrist rehabilitation equipment

II. A. Structural design

The wrist joint, which serves as a bridge between the hand and the forearm, is a complex multicompartmental joint. The wrist joint is composed of the navicular, lunate, triangular, bean, major polygonal, minor polygonal, capitate and hook bones, which together form the radial carpal, intercarpal and metacarpal carpometacarpal joints.

The wrist joint is a composite joint with two degrees of freedom, and its movements can be broken down into two groups: palmar flexion/posterior extension and radial flexion/ulnar flexion. In people's daily life, the palmar flexion/posterior extension degree of freedom of the wrist joint is often used, so this paper takes this degree of freedom as a representative for research.

Based on the above biological characteristics of the human wrist joint, this paper designs a wrist rehabilitation device. The device adopts a rotating joint J_6, which can realize the palmar flexion/posterior extension movement around J_6 to complete the wrist joint movement. The sliding handle structure can facilitate the immobilization of the patient's palm, and the combination of different components can ensure a better fit of the patient's wrist module wear.

II. B. Control systems

In order to realize the automation and standardization of this equipment in the process of rehabilitation therapy, there is an urgent need to design a suitable and efficient control system. This paper focuses on the analysis of the hardware structure of the control system and software design of the two modules.

(1) Control system hardware design

In this paper, the master-slave control system with separate control and centralized management is selected, and the modularization concept of this system responds to the demand for diversified equipment performance. Among them, the master controller executes the task decision-making commands, and the slave controller controls according to the commands. Its hardware structure is shown in Figure 1.

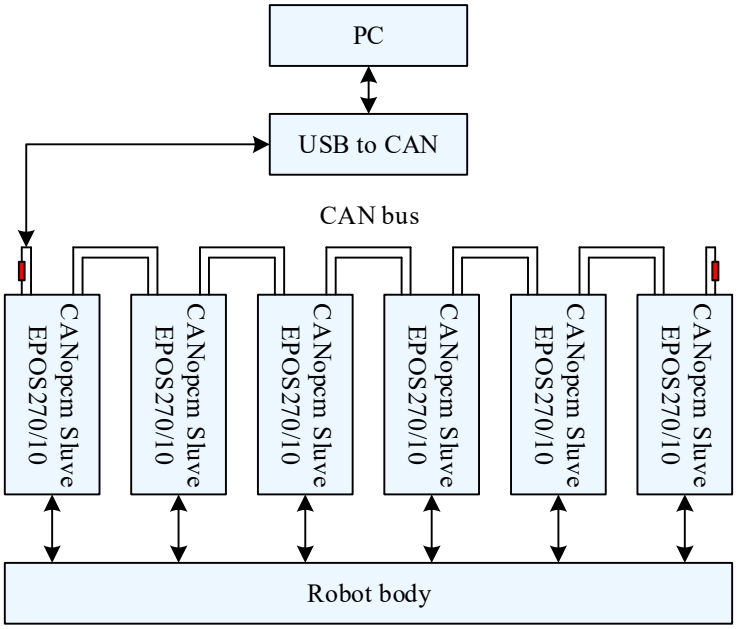

Figure 1: Hardware structure of the control system

The hardware structure of the device can be divided into three parts, which are upper hardware PC, CAN bus and lower hardware device body. Among them, the upper hardware PC manipulates the motion mode of the device; the lower hardware device body is mainly composed of six groups of servo systems, each servo system is composed of brushless DC motors and actuators, and supports communication such as USB, RS232 and CAN bus; because of the anti-interference and real-time characteristics of CAN bus communication, the upper and lower layers of the hardware structure choose to use this communication method. Because of the anti-interference and real-time characteristics of CAN bus communication, the upper and lower layers of this hardware structure choose to use this communication method, using the CANopen protocol of the OSI application layer. The upper layer of the PC and the CAN bus also add a USB to CAN expansion card, the role of which is used to expand the communication

capacity, the expansion card can minimize the delay and low power consumption to achieve high speed, no loss of message transmission.

(2) Control system software design

In view of the modularity of the control system of the device and the characteristics of high portability, this paper selects the ROS-based operating system platform that contains many function library functions. This platform is built on a PC by the ubuntu16.04 and ROS unified composition, its software design framework shown in Figure 2.

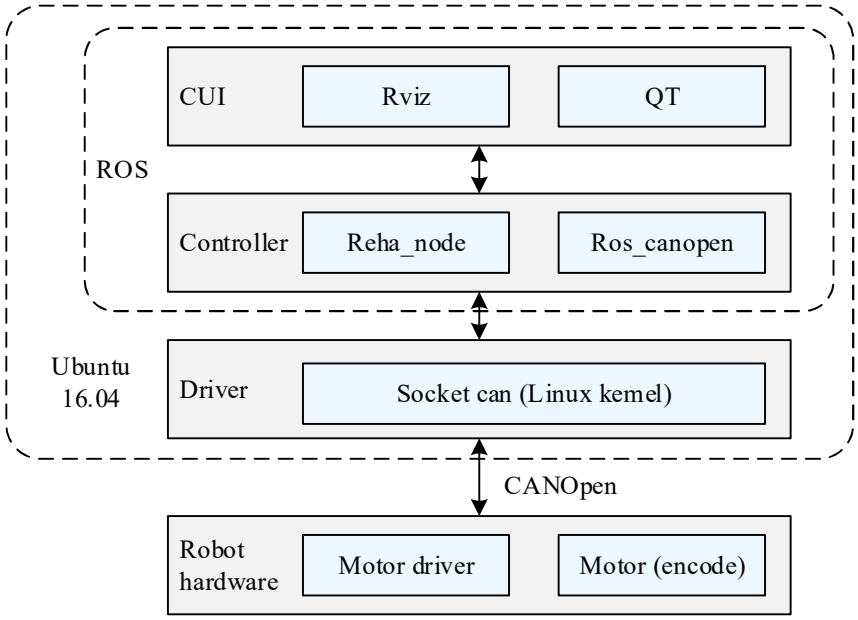

Figure 2: Control system software framework

The software framework of the device can also be decomposed into three parts: GUI layer, Controller layer and Driver layer. Among them, the first GUI layer mainly uses Rviz and QT libraries to develop a visual human-computer interaction interface; the designed interface can be passed to the second Controller layer by manually inputting commands, and the Reha_node and ros_canopen nodes contained in the Controller layer are mainly responsible for driving the reconfigurable robot to realize the selected trajectory and motion. The Reha_node and ros_canopen nodes in the Controller layer are mainly responsible for driving the reconfigurable robot to realize the selected trajectory, and the ros_canopen node realizes the communication between ROS and the driver under the CANopen protocol; in the third layer, Driver layer, we use the USB to CAN communication card to set up the CAN communication network with the driver. In the Robot hardware layer, the encoder of the motor provides real-time feedback of the joint motion information, so that the current state of the model can be observed in the interactive interface in real time.

III. SEMG-based motion intention recognition

Muscle force and joint moment can reflect the specific physiological information of the muscles and joints of the patient during the rehabilitation process, which can make a quantitative assessment of the rehabilitation status of the patient and also provide an effective amount of interaction control to the wrist rehabilitation equipment. In order to ensure the accuracy of elbow and wrist multi-joint motion intention recognition, the signal characteristics of sEMG signals are fully integrated, and the recognition and analysis work of elbow and wrist joint motion intentions are carried out at the muscle and skeletal joint levels respectively.

III. A. Acquisition and pre-processing of surface EMG signals

III. A. 1) Signal pre-processing

In general, the acquisition process of raw EMG signals tends to mix some impurity signals, in order to be more effective in the subsequent analysis of the acquired data, it is necessary to first preprocess the raw signal of sEMG to filter out the noise. The processing steps are described below:

(1) In order to eliminate motion artifacts and baseline offsets in the signal, a 4th order Butterworth high-pass filter is adopted for high-pass filtering, in which the cutoff frequency is selected to be 25 Hz;

(2) In this paper, a non-negative matrix decomposition algorithm is planned to be used for data extraction, and since the algorithm demands that the matrix possesses non-negative properties, full-wave rectification of the sEMG is required so that the signal satisfies the non-negative provision and meets the muscular activity level in physiology;

(3) In order to effectively reduce the potential impact of the amplitude difference of sEMG among different individuals on the analysis of muscle coordination, the sEMG also needs to be normalized;

(4) In order to eliminate the effects caused by high-frequency noise, a 4th-order Butterworth low-pass filter was selected to accomplish the envelope extraction of the signal, where the cutoff frequency was chosen to be 3 Hz.

Given that future work will involve the need for real-time signal processing, in order to simplify the computational process and improve efficiency, this study adopts an intuitive and simple numerical normalization method. This is done by performing the normalization by dividing each data point in the sample by the maximum absolute value of all the values in that sample data set:

$$data = \frac{x}{|\max|} \tag{1}$$

where $\max$ is the maximum value and x is the sample data.

III. A. 2) Calculation of muscle activation

During joint movement, the variable indicating muscle activity is actually a non-negative number in the range of 0-1, where the number 0 means that the muscle is in an inactive state, and the number 1 means that the muscle is in a state of complete activation. The normalized EMG signal does not directly label the degree of muscle activity, and it is necessary to first calculate the intensity of neural activity $u(t)$ based on the normalized EMG signal, as in Eq:

$$u_j(t) = \alpha e_j(t-d) - \beta_1 u_j(t-1) - \beta_2 u_j(t-2) \tag{2}$$

Eq, α - gain coefficient, d - time delay of electrodes, β_1, β_2 - recurrence coefficients.

And the three coefficients α, β_1 and β_2 in the above equation must also satisfy the following conditions:

$$\begin{cases} \alpha = \beta_1 + \beta_2 \\ \beta_1 = C_1 + C_2 \\ \beta_2 = C_1 \cdot C_2 \end{cases} \tag{3}$$

In this recursive model, $|C_1|<1, |C_2|<1$. A given neural activation strength $u(t)$ is not only related to its performance at the current moment, but also closely related to the neural activation strengths $u(t-1)$, $u(t-2)$ at the previous two time points. In order to accurately simulate and predict the dynamics of neural activation, this model also takes into account the natural delay time of the electrode detection signal, and usually, the electrode delay time d is generally taken as 10ms.

After obtaining the nerve activation strength $u(t)$, the more commonly used nonlinear model is chosen to be used to solve the muscle activation $a(t)$, as shown in equation (4):

$$a_j(t) = \frac{e^{Au_j(t)} - 1}{e^A - 1} \tag{4}$$

where A indicates the degree of nonlinearity, its range of values is generally restricted to -3 to 0. When the value of A tends to 0, it indicates the existence of a strong nonlinear connection; conversely, if the value approaches -3, it indicates that these interactions are closer to a linear relationship. The actual value of A is usually determined by the adjustment process. In this paper, the value of A is set to -1.2.

With the above settings and processing, it was possible to complete the entire process of analyzing the raw EMG signals collected from the sEMG and then solving the muscle activation degree.

III. B. LSSVM-based finger-wrist motion intention recognition

III. B. 1) Basic calculation process

LSSVM is different from the classification method of traditional SVM, which adopts the least squares linear system as the loss function instead of the traditional quadratic programming method, which reduces the computational complexity and improves the processing speed, and at the same time, it also has a high recognition rate and a good generalization ability, and the computing speed is significantly better than other SVM methods. The basic computational process is as follows, optimizing the problem as an equation constraint:

$$\begin{aligned} &\min_{w,b,e} J(w,e) = \frac{1}{2} w^T w + \frac{1}{2} \gamma \sum_{k=1}^{N} e_k^2 \\ &s.t. y_k \left[w^T \phi(x_k) + b \right] = 1 - e_k, k = 1, \ldots, N \end{aligned} \tag{5}$$

Construct the Lagrange function to transform the original problem into a problem of finding the maximum value of α :

$$L(w,b,e;\alpha) = J(w,e) - \sum_{k=1}^{N} \alpha_k \left\{ y_k [w^T \varphi(x_k) + b] - 1 + e_k \right\} \tag{6}$$

obtained by taking the partial derivatives of the four variables and equating them all to zero:

$$\begin{cases} w = \sum_{k=1}^{N} \alpha_k y_k \varphi(x_k) \\ \sum_{k=1}^{N} \alpha_k y_k = 0 \\ \alpha_k = \gamma e_k, k = 1, \ldots, N \\ y_k [w^T \varphi(x_k) + b] - 1 + e_k = 0, k = 1, \ldots, N \end{cases} \tag{7}$$

From the above a system of linear equations is presented:

$$\begin{bmatrix} 0 & y^T \\ y & \Omega + I / y \end{bmatrix} \begin{bmatrix} b \\ \alpha \end{bmatrix} = \begin{bmatrix} 0 \\ l_v \end{bmatrix} \tag{8}$$

where Ω is called the kernel matrix:

$$\begin{aligned} \Omega_{kl} &= y_k y_l \varphi(x_k)^T \varphi(x_l) \\ &= y_k y_l K(x_k, x_l), k, l = 1, \ldots, N \end{aligned} \tag{9}$$

By solving the above system of equations, a set of a and b can be obtained. the LSSVM classification expression is:

$$y(x) = sign\left[\sum_{k=1}^{N} \alpha_k y_k K(x, x_k) + b \right] \tag{10}$$

During the design process, the penalty factor γ and the parameter σ in the kernel function play a decisive role in the prediction performance.

III. B. 2) Hyperparameter optimization strategy

The two hyperparameters γ and σ in LSSVM are empirically pre-set fixed values, which are determined at the beginning of the design of the algorithm, but since the hyperparameters γ and σ play a decisive role in the prediction performance, the use of the fixed pre-set values may reduce the generalization ability of the classifier, which in turn affects the recognition accuracy, especially in the finger-wrist movement intention recognition. In order to improve the adaptability to different individuals and optimize the classification effect, an optimization algorithm is used to optimize the two hyperparameters in LSSVM.

In this paper, the weighted variate particle swarm algorithm (WVPSO) is used to optimize the hyperparameters in LSSVM to further improve the recognition accuracy and generalization ability of LSSVM. The traditional particle swarm algorithm (PSO) belongs to intelligent optimization algorithms, and its core concept is to find the optimal solution through the cooperation and information exchange among individuals in the group, but there are some shortcomings, such as easy to fall into premature maturity, low convergence accuracy, slow convergence speed in the later stage, and so on, and the WVPSO algorithm is optimized on this basis, and it shows superior performances in terms of the solution accuracy and convergence speed. WVPSO algorithm is optimized on the basis of this algorithm, which shows superior performance in terms of solution accuracy and convergence speed.

The standard PSO algorithm begins by initializing to a population of random particles, each of which symbolizes a potential solution to a given problem, i.e., the 2 hyperparameters γ and σ in the LSSVM are used as random particles. We envision a population of N particles together in a search space with D dimensions, where the i th particle is denoted as a D -dimensional vector:

$$X_i = (x_{i1}, x_{i2}, \ldots, x_{iD}), i = 1, 2, \ldots, N \tag{11}$$

The hyperparameters γ and σ are preferred for the LSSVM in this optimization, so that the value of D is 2 and N is set to 20. The velocity of the i th particle is denoted as:

$$V_i = (v_{i1}, v_{i2}, \ldots, v_{iD}), i = 1, 2, \ldots, N \tag{12}$$

The optimal position currently searched by the i th particle is called the individual optimum:

$$P_{best} = (p_{i1}, p_{i2}, \ldots, p_{iD}), i = 1, 2, \ldots, N \tag{13}$$

The optimal position currently searched by the entire population is called the population optimum:

$$g_{best} = (p_{g1}, p_{g2}, \ldots, p_{gD}), i = 1, 2, \ldots, N \tag{14}$$

The i th particle can update its velocity and position according to the following equation:

$$\begin{aligned} v_{id} &= \omega \times v_{id} + c_1 r_1 (p_{id} - x_{id}) + c_2 r_2 (p_{gd} - x_{id}) \\ x_{id} &= x_{id} + v_{id} \end{aligned} \tag{15}$$

where ω is the inertia weight, c_1 and c_2 are the learning factors, and r_1 and r_2 are random numbers between 0 and 1.

The WVPSO optimization algorithm is tuned by adjusting the weights ω, learning factors c_1 and c_2 in order to ensure that the algorithm maintains a strong global search capability while balancing the local search capability in pursuing the optimization strategy:

$$\begin{aligned} \omega &= 0.8 \times \exp\left(\frac{-2.5it}{MaxIt}\right) \\ c_1 &= c_{1up} - rand \times \left(1 - \exp\left(\frac{-MaxIt}{MaxIt - it}\right)\right) \times (c_{1up} - c_{1low}) \\ c_2 &= c_{2low} + rand \times \left(1 - \exp\left(\frac{-MaxIt}{MaxIt - it}\right)\right) \times (c_{2up} - c_{2low}) \end{aligned} \tag{16}$$

where, it is the current iteration number, $MaxIt$ is the maximum iteration number; $rand$ is a random number between 0-1; c_{1up}, c_{1low} are upper and lower bounds of the self-learning factor, respectively; c_{2up}, c_{2low} are upper and lower bounds of the group learning factor, for this optimization.] are the upper and lower bounds of the population learning factor, respectively. For this optimization, here, $MaxIt$ is set to 20, c_{1up} and c_{1low} are set to 2.5 and 0.5, respectively; c_{2up} and c_{2low} are set to 3.5 and 0.8, respectively.

In order to enrich the diversity of the particle population and improve the search accuracy of the algorithm, the WVPSO algorithm dynamically adjusts the positions and velocities of the particles by introducing a weighted mutation strategy that combines the arithmetic crossover and the natural selection mechanism after each evaluation of the fitness. Regarding the proportion of mutated particles, they are selected in the following way:

$$\left[|P_1|, |P_2|, \ldots, |P_N|\right] \tag{17}$$

$$\left[\underbrace{|P_1|, |P_2|, \ldots, |P_{\xi_1}|}_{\xi_1}, \underbrace{|P_{\xi_1+1}|, \ldots, |P_{\xi_2}|}_{\xi_2}, \underbrace{|P_{\xi_2+1}|, \ldots, |P_{\xi_3}|}_{\xi_3}, \underbrace{|P_{\xi_3+1}|, \ldots, |P_{\xi_4}|}_{\xi_4}, \ldots, |P_N|\right] \tag{18}$$

The absolute values of the adaptation values of all particles are first arranged in order from smallest to largest by Eq. (17) and subsequently partitioned by Eq. (18). The arithmetic crossover formula is as follows:

$$\begin{aligned} x_{\xi_3} &= rand \times x_{\xi_2} + (1 - rand) \times x_{\xi_3} \\ v_{\xi_3} &= rand \times v_{\xi_2} + (1 - rand) \times v_{\xi_3} \end{aligned} \tag{19}$$

where x_{ξ_2} and x_{ξ_3} are the positions of the particles at ξ_2 and ξ_3 in Eq. (18); and v_{ξ_2} and v_{ξ_3} are the velocities of the particles at ξ_2 and ξ_3 in Eq. (18); and $rand$ is a random number between 0 and 1. The natural selection process is as follows:

$$\begin{cases} x_{\xi_4} = x_{\xi_1} \\ v_{\xi_4} = v_{\xi_1} \end{cases} \tag{20}$$

where x_{ξ_1} and x_{ξ_4} are the positions of the particles at ξ_1 and ξ_4 in Eq. (17), and v_{ξ_4} and v_{ξ_4} are the velocities of the particles at ξ_1 and ξ_4 in equation (18). Finally, in order to solve the problem that the algorithm tends to converge to the local optimal solution too early, Gaussian perturbation is introduced when the algorithm falls into premature maturity, which prompts the particles to jump out of the current local optimal region, thus increasing the possibility of global search.

IV. Analysis of the effect of digital wrist rehabilitation equipment based on multi-sensor fusion technology

In this paper, 50 cases of chronic wrist dysfunction patients (disease duration ≥6 months) in the rehabilitation department of cooperative hospitals were selected as research subjects, and they were divided into the control group (n=25) and the experimental group (n=25) according to the random number table method. The general information of the two groups was comparable, and the difference was not statistically significant (P>0.05). The

study was approved by the Medical Ethics Committee, and the patients and their families gave informed consent and signed the informed consent form.

IV. A. Synchronized Signal Acquisition and Signal Preprocessing

According to the theory of skeletal and muscular anatomy of the upper limb, the subjects use the wrist rehabilitation equipment for rehabilitation training mainly for flexion/extension of the shoulder, elbow and wrist joints, in which shoulder flexion/extension is mainly accomplished by contraction/relaxation of the deltoid and other muscles. Elbow flexion/extension is dependent on the triceps and biceps muscles. Wrist flexion/extension is mainly accomplished by the cooperation of synergistic muscles such as radial wrist extensor and radial wrist flexor. Therefore, this experiment mainly collects the surface electromyographic signals of upper limb deltoid anterior fasciculus, deltoid posterior fasciculus, triceps brachii, biceps brachii, radial wrist extensors, and radial wrist flexors, as well as information on the angle of joint motion during shoulder, elbow, and wrist flexion/extension. According to the data acquisition step, electrode sheets were sequentially pasted on the surface of the relevant muscles along the direction of the muscle fibers, with a distance of 2-3 cm between each pair of electrode sheets, and the surface EMG signals of the multiple muscles and the joint motion information were synchronously acquired using the BIOPAC physiological signal acquisition system and the inertial sensor.

In surface EMG signal acquisition, the signal will inevitably be interfered by noise, thus affecting the accuracy of motion intention recognition. According to the surface EMG signal processing technique in section 3.1, the 6-channel surface EMG signal was preprocessed, and the surface EMG signals of a certain subject before and after preprocessing were shown in Fig. 3 (a~c), and the digital filter filtered out the high-frequency unwanted signals as well as the low-frequency interferences, and preserved the energy of the EMG signal. The digital filter filtered out high-frequency useless signals and low-frequency interferences, and retained the energy of EMG signals. At the same time, the full-wave rectification technique was utilized to ensure data smoothing and reduce data oscillation. It can be clearly seen that the subject's muscles contracted/relaxed periodically as the human upper limb moved at a uniform speed, and the amplitude of the surface EMG signals increased/decreased in a cyclical manner. During the upper limb flexion/extension movement, the collected muscles are active and antagonist muscles, therefore, with the joint flexion/extension, the active muscles contract/relax and the antagonist muscles relax/contract, and the surface EMG signals are in a complementary state.

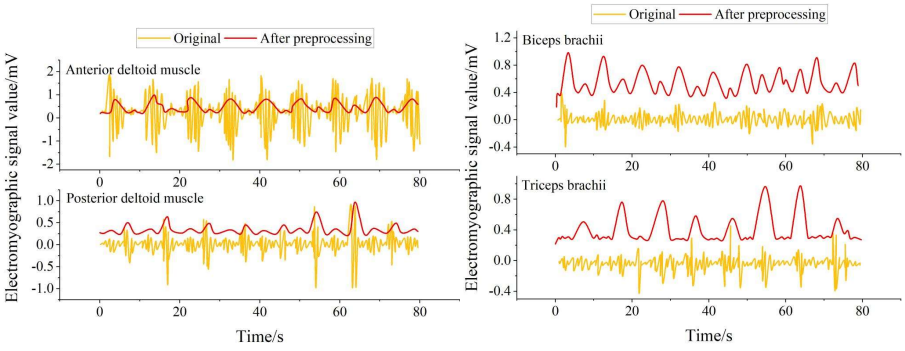

(a)Shoulder joint

(b)Elbow joint

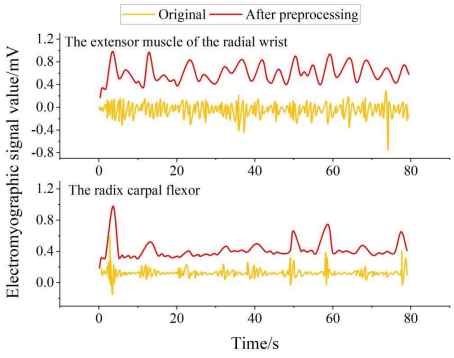

(c)Wrist joint

Figure 3: Surface electromyography signals before and after pretreatment

IV. B. Analysis of simulation results

In order to verify the correctness of the theoretical model and the reasonableness of the design scheme, the designed digital wrist rehabilitation equipment is further studied. The simulation model of the wrist rehabilitation equipment is established based on ADAMS simulation software, and virtual prototype simulation is carried out. After the simulation is completed, the simulation curves obtained are compared and analyzed in detail with the theoretical numerical curves to verify the accuracy and reliability of the theoretical model.

The torque variation curves of the torsion spring at the elbow and wrist joints in the wrist rehabilitation device in one cycle are shown in Fig. 4. It is known that the torque of the torsion spring is mainly related to its own stiffness and rotation angle, and the torsion spring has a certain stiffness, the curve has a high degree of consistency with the trend of the curve obtained based on the theoretical model of kinematics, which further verifies that the wrist rehabilitation device is consistent with the movement of the human upper limb during the movement of the upper limb of the human body, i.e., it can be perfectly adapted to the human body, and it does not cause any interference in the human body's movement.

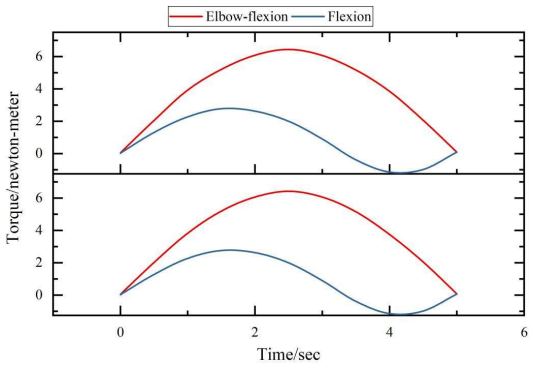

Figure 4: Torque variation curve

The height change curve of the model end point relative to the bottom end obtained from the simulation model of the wrist rehabilitation equipment is shown in Figure 5. Comparing the simulation curve with the height change curve of the end point of the model obtained based on the kinematic theory model, the two curves are basically the same in terms of numerical size and the change trend is basically the same. It can be observed that the end height first decreases and then increases, and there is a certain deformation, in line with the kinematic theory model of the law of motion. Since the two curves are smooth and gentle with no sudden changes, it can be further proved that the wrist rehabilitation equipment does not interfere with the movement of the human upper limb after wearing.

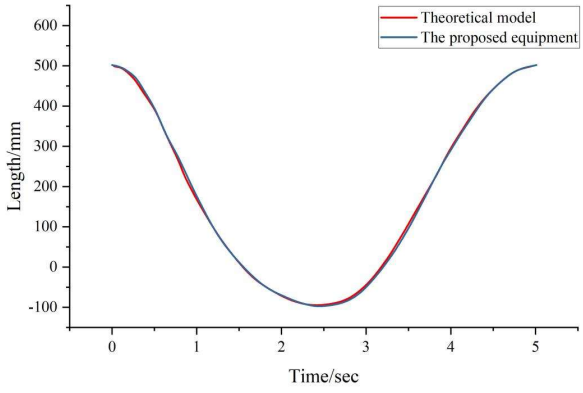

Figure 5: Simulation curves of torque changes in elbow and wrist joints

The moment change curves of the elbow and wrist joints obtained by the simulation model of the wrist rehabilitation equipment are shown in Figure 6. Through observation, the comparison between the simulation curve and the moment change curve obtained from the theoretical model can be found that the two curves are basically the same in numerical magnitude, and the change trend is highly consistent, which further verifies the reasonableness of the design of the wrist joint rehabilitation equipment.

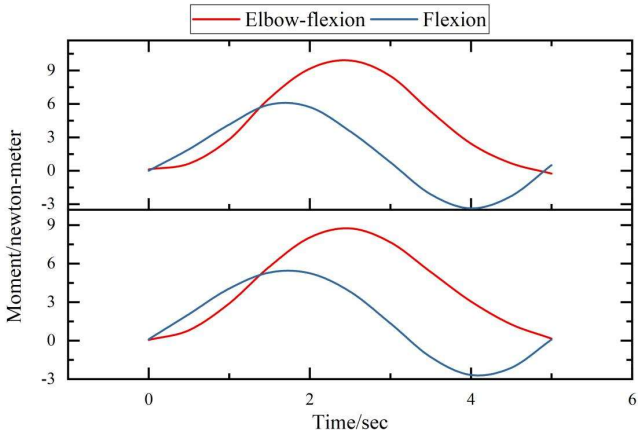

Figure 6: The torque variation curves of the elbow and wrist joints

IV. C. Analysis of application effects

The experimental group used the equipment proposed in this paper to carry out rehabilitation training after completing the treatment, and the control group carried out conventional rehabilitation training after completing the treatment, and the course of both groups was 6 weeks. At the end of the experiment, the follow-up was 3 months to evaluate the treatment effect of the two groups. Wrist function was evaluated from four aspects, namely, pain grip strength, function, dorsal extension/palmar flexion mobility, with scores ranging from 0 to 25, and the scores were positively correlated with the function. Quality of life was evaluated in both groups using the short form of health survey (SF-36), only 4 aspects of physical, somatic, emotional, and social were selected, and the scores were 0~100, and the scores were positively correlated with the quality of life.

SPSS25.0 software was used to statistically analyze the obtained data. Measurement data were expressed as (M±SD), and independent sample t-test was used for inter-group comparison, and paired t-test was used for intra-group comparison. Count data were expressed as rate (%), and χ^2 test was used for comparison, and the difference was statistically significant at P<0.05.

The results of the comparison of wrist joint function before and after treatment between the two groups are shown in Table 1. Before treatment, there was no statistically significant difference between the two groups in terms of wrist joint function (P>0.05). After treatment, the pain, grip strength, function, and dorsal extension/palmar flexion mobility scores of the two groups were improved compared with those before treatment, and the mean values of the experimental group were higher than those of the control group by 3.09, 2.41, 4.01, and 3.84 points, respectively, and the differences were statistically significant (P<0.05).

Table 1: Results of comparison of wrist function(M±SD)

		Experimental group	Control group	t value	P value
Pain	Before	10.34±1.08	10.32±1.12	0.099	0.836
	After	20.57±1.11*	17.48±1.42*	11.873	<0.001
Grip strength	Before	11.47±1.39	11.46±1.08	0.077	0.873
	After	19.66±1.47*	17.25±1.73*	9.376	<0.001
Function	Before	10.86±1.13	10.85±1.15	0.028	0.902
	After	20.83±1.03*	16.82±1.38*	15.422	<0.001
Dorsiflexion/Flexion range of motion	Before	10.47±1.08	10.45±1.12	0.086	0.917
	After	20.63±1.03*	16.79±1.35*	15.386	<0.001

The results of the comparison of quality of life between the two groups before and after treatment are shown in Table 2. Before treatment, there was no statistically significant difference in the quality of life between the two groups (P>0.05). After treatment, the physical, somatic, and emotional-social scores of the two groups were improved compared with those before treatment, and the mean values of the experimental group were higher than those of the control group by 8.71, 9.01, 9.83, and 9.32 points, respectively, and the differences were statistically significant (P<0.05).

Table 2: Comparative quality of life results(M±SD)

		Experimental group	Control group	t value	P value
Physiology	Before	60.29±2.97	60.28±2.74	0.074	0.849
	After	89.37±2.18*	80.66±2.56*	12.684	<0.001
Body	Before	58.38±2.52	58.38±2.54	0.038	0.938
	After	90.17±2.33*	81.16±2.23*	14.973	<0.001
Emotion	Before	59.91±2.28	59.89±2.31	0.096	0.882
	After	89.94±2.37*	80.11±2.75*	15.992	<0.001
Society	Before	60.37±2.16	60.35±2.35	0.091	0.917
	After	90.38±2.64*	81.06±2.47*	15.275	<0.001

V. Conclusion

In this paper, a wrist rehabilitation device based on multi-sensor fusion technology is designed to explore its practical effect by combining simulation experiments and practical verification.

The simulation curves obtained from the simulation model are highly consistent with the theoretical numerical curves, proving the correctness of the design of this paper. Putting the equipment into use, after treatment, the pain, grip strength, function, dorsal extension/palmar flexion mobility scores of the experimental group and the control group were improved compared with those before treatment, and the mean values of the experimental group were higher than those of the control group by 3.09, 2.41, 4.01, and 3.84 points, respectively, and the differences were statistically significant (P<0.05). Physical, somatic and emotional-social scores of the two groups were improved compared with the pre-treatment, and the mean values of the experimental group were higher than those of the control group by 8.71, 9.01, 9.83 and 9.32 points, respectively, and the difference was statistically significant (P<0.05). The experiment proved the rationality of the design of the wrist rehabilitation equipment, which can effectively help patients to complete the rehabilitation training.

References

[1] Kong, L., Peng, X., Chen, Y., Wang, P., & Xu, M. (2020). Multi-sensor measurement and data fusion technology for manufacturing process monitoring: a literature review. International journal of extreme manufacturing, 2(2), 022001.

[2] Tong, Y., Bai, J., & Chen, X. (2020, October). Research on multi-sensor data fusion technology. In Journal of Physics: Conference Series (Vol. 1624, No. 3, p. 032046). IOP Publishing.

[3] Zhang, Y., Zhang, B., Shen, C., Liu, H., Huang, J., Tian, K., & Tang, Z. (2024). Review of the field environmental sensing methods based on multi-sensor information fusion technology. International Journal of Agricultural and Biological Engineering, 17(2), 1-13.

[4] Weishi, C. H. E. N., Yifeng, H., & Xianfeng, L. U. (2020). Survey on application of multi-sensor fusion in UAV detection technology. Modern radar, 42(6), 15-29.

[5] Elsanhoury, M., Koljonen, J., Välisuo, P., Elmusrati, M., & Kuusniemi, H. (2021, September). Survey on recent advances in integrated GNSSs towards seamless navigation using multi-sensor fusion technology. In Proceedings of the 34th international technical meeting of the satellite division of the institute of navigation (ION GNSS+ 2021) (pp. 2754-2765).

[6] Chen, M., Cai, Z., Zeng, Y., & Yu, Y. (2023). Multi-sensor data fusion technology for the early landslide warning system. Journal of Ambient Intelligence and Humanized Computing, 14(8), 11165-11172.

[7] Wang, Z., Wu, Y., & Niu, Q. (2019). Multi-sensor fusion in automated driving: A survey. Ieee Access, 8, 2847-2868.

[8] Yeong, D. J., Velasco-Hernandez, G., Barry, J., & Walsh, J. (2021). Sensor and sensor fusion technology in autonomous vehicles: A review. Sensors, 21(6), 2140.

[9] Wang, X., Li, K., & Chehri, A. (2023). Multi-sensor fusion technology for 3D object detection in autonomous driving: A review. IEEE Transactions on Intelligent Transportation Systems, 25(2), 1148-1165.

[10] Lin, K., Li, Y., Sun, J., Zhou, D., & Zhang, Q. (2020). Multi-sensor fusion for body sensor network in medical human–robot interaction scenario. Information Fusion, 57, 15-26.

[11] Muzammal, M., Talat, R., Sodhro, A. H., & Pirbhulal, S. (2020). A multi-sensor data fusion enabled ensemble approach for medical data from body sensor networks. Information Fusion, 53, 155-164.

[12] Fortino, G., Ghasemzadeh, H., Gravina, R., Liu, P. X., Poon, C. C., & Wang, Z. (2019). Advances in multi-sensor fusion for body sensor networks: Algorithms, architectures, and applications. Inf. Fusion, 45, 150-152.

[13] Zhang, D. (2021). Interoperability technology of sports health monitoring equipment based on multi-sensor information fusion. EURASIP Journal on Advances in Signal Processing, 2021(1), 62.

[14] Feng, R., Geng, Z., Li, A., Chu, Y., Wu, C., Zhang, N., ... & Tang, F. (2021). Noninvasive blood glucose monitor via multi-sensor fusion and its clinical evaluation. Sensors and Actuators B: Chemical, 332, 129445.

[15] Eschweiler, J., Li, J., Quack, V., Rath, B., Baroncini, A., Hildebrand, F., & Migliorini, F. (2022). Anatomy, biomechanics, and loads of the wrist joint. Life, 12(2), 188.

[16] Laulan, J., Marteau, E., & Bacle, G. (2015). Wrist osteoarthritis. Orthopaedics & Traumatology: surgery & research, 101(1), S1-S9.

[17] Obert, L., Loisel, F., Jardin, E., Gasse, N., & Lepage, D. (2016). High-energy injuries of the wrist. Orthopaedics & Traumatology: Surgery & Research, 102(1), S81-S93.

[18] Andersson, J. K., Hagert, E., & Brittberg, M. (2021). Cartilage injuries and posttraumatic osteoarthritis in the wrist: a review. Cartilage, 13(1_suppl), 156S-168S.
[19] Liu, P., & Hu, Y. (2025). Construction and analysis of digital intelligent flexible wrist rehabilitation equipment. J. COMBIN. MATH. COMBIN. COMPUT, 127, 7879-7898.
[20] Costa, F., Janela, D., Molinos, M., Moulder, R. G., Lains, J., Francisco, G. E., ... & Correia, F. D. (2022). Digital rehabilitation for hand and wrist pain: a single-arm prospective longitudinal cohort study. Pain Reports, 7(5), e1026.
[21] Duy, C. V. (2024). Design and development of a wrist rehabilitation device with an interactive game. Results in Engineering, 22, 102336.
[22] Kabir, R., Sunny, M. S. H., Ahmed, H. U., & Rahman, M. H. (2022). Hand rehabilitation devices: A comprehensive systematic review. Micromachines, 13(7), 1033.